Longitudinal Stability Augmentation of Seaplanes in Planing

Keiichi Ito* and Tom Dhaene†
Ghent University, 9050 Ghent, Belgium
Yoshiaki Hirakawa‡ and Tsugukiyo Hirayama§
Yokohama National University, Yokohama 240-8501, Japan
and
Tatsumi Sakurai¶
Hiyoh Aircraft Manufacturing and Development Company, Tokyo 142-0041, Japan

DOI: 10.2514/1.C033588

The towing tank experiments conducted at Yokohama National University from November 30 to December 9 in 2005 suggested a new way of suppressing a dangerous coupled motion between heave and pitch called porpoising. The research in this paper was developed on the observations made in the experiments and conducted numerical simulations to further investigate the parametric design space. Two linear-time-invariant models were developed: rigid-body planing craft (conventional float planes or flying boats), and flexibly supported planing craft. The latter could simulate the new method found in the experiments for suppressing porpoising. In this study, the stability of the oscillatory motions was analyzed to see the effect of design variables on the inception of porpoising. The parametric study of flexibly supported float planes in the context of porpoising was a new contribution in the conceptual design of seaplanes.

Nomenclature

a	=	distance between center of gravity and R_v (positive when pitch-down moment results), m
a_{33}	=	two-dimensional added mass of a wedge plunging into water, kg/m
A_{ij}	=	hydrodynamic added mass/moment of inertia in the direction of i due to the motion in the direction of j
AHR	=	average hull roughness, μm
B	=	beam length (i.e. width) of a float, m
B_{ij}	=	hydrodynamic damping coefficient in the direction of i due to the motion in the direction of j
c	=	pitching moment arm of hydrodynamic resultant pressure force N with respect to center of gravity (positive when pitch-down moment results), $l_{\text{cg}} - l_p$
C_F	=	friction coefficient
$c_{f,b}$	=	damping coefficients in the flexible support (front and back), Ns/m
C_{ij}	=	hydrodynamic restoring force/moment coefficient in the direction of i due to the motion in the direction of j
C_{L_0}	=	lift coefficient for zero deadrise angle ($\beta = 0$ rad)
C_{L_β}	=	lift coefficient
d	=	draft, m
f	=	thrust line distance from center of gravity (positive when pitch-up moment results), m
F_{L_0}	=	lift force for zero deadrise angle ($\beta = 0$ rad)
F_{L_β}	=	lift force
F_{n_B}	=	Froude number based on the beam length
I_A	=	pitching mass moment of inertia of the aircraft without the floats for the flexible-support model, kg/m^2
I_B	=	pitching mass moment of inertia of the floats for the flexible-support model, kg/m^2
I_{55}	=	pitching mass moment of inertia of rigidly supported seaplane/model, kg/m^2
$k_{f,b}$	=	spring constants in the flexible support (front and back), N/m
L_C	=	wetted chine length measured from the step, m
L_K	=	wetted keel length measured from the step, m
l_p	=	distance measured along the keel from the step to the center of hydrodynamic pressure, m
$l_{Af,Ab}$	=	attachment locations of flexible supports on the aircraft relative to center of gravity of the aircraft, m
$l_{Bf,Bb}$	=	attachment locations of flexible supports on the floats relative to center of gravity of the floats, m
l_{cg}	=	longitudinal distance of center of gravity along the keel line measured from the step or transom, m
M	=	mass of the aircraft for the rigid body model, kg
m_A	=	mass of the aircraft for the flexible-support model, kg
m_B	=	mass of the float for the flexible-support model, kg
N	=	resultant hydrodynamic pressure force acting on the planing surface, N
N_f	=	number simulation function calls
N_s	=	number of simulation function calls that satisfied the stability criteria
R_n	=	Reynolds number, UL_K/ν
R_ν	=	frictional force acting on the planing hull assumed to act parallel to keel line, N
T	=	thrust force, N
t	=	time, s
U	=	planing speed, m/s
V	=	vertical velocity with which the hull impacts the water surface, $U \tan \tau$
vcg	=	vertical distance of center of gravity from the keel line, m
x_a, z_a	=	inertial coordinate moving with the aircraft's CG's equilibrium position without floats, x_a pointing horizontally to the stern, z_a pointing vertically upward

Received 12 June 2015; revision received 20 November 2015; accepted for publication 16 January 2016; published online 24 May 2016.

*Researcher, Department of Information Technology (INTEC), iMinds, Gaston Crommenlaan 8 bus 201, Ledeberg; also Technical Specialist, Noesis Solutions, Gaston Geenslaan 11 B4, 3001 Leuven, Belgium. Student Member AIAA.

†Professor, Department of Information Technology (INTEC), iMinds, Gaston Crommenlaan 8 bus 201, Ledeberg.

‡Associate Professor, Department of System Integration, 79-5, Tokiwadai, Hodogayaku, Kanagawa.

§Professor Emeritus, Department of System Integration, 79-5, Tokiwadai, Hodogayaku, Kanagawa.

¶Director, 1-7-1, Togoshi, Shinagawaku.

x_b, z_b = inertial coordinate moving with the aircraft's CG's equilibrium position when the supports are rigid and moving along the floats' CG's equilibrium position when the supports are flexible, x_b pointing horizontally to the stern, z_b pointing vertically upward
$z_{\max}$ = height above the undisturbed water surface where the maximum pressure on the V-shaped hull happens due to its impact to the water
β = deadrise angle, rad
$\beta_{\deg}$ = deadrise angle, deg
ϵ = thrust line angle with respect to the keel line (positive upwards), rad
η_3, η_5 = displacement in heave and pitch respectively from the inertial coordinate x_b, z_b
λ_0 = λ_W at the static equilibrium position
λ_W = mean wetted length to beam ratio, $0.5(L_K + L_C)/B$
$\mathcal{R}(\sigma)_{\max}$ = maximum real part of the eigenvalues of a matrix $\boldsymbol{K}$ as in $\dot{\boldsymbol{x}} = \boldsymbol{K}\boldsymbol{x}$, 1/s
ρ = water density, kg/m^3
τ = trim angle of planing area, rad
$\tau_{\deg}$ = trim angle of planing area, deg
ξ_3, ξ_5 = displacement in heave and pitch respectively from the inertial coordinate x_a, z_a

I. Introduction

SEAPLANES and their amphibian versions have largely been a neglected type of aircraft in recent aviation, except for very specific missions and in limited geographic regions. This is due to higher maintenance costs, less payload, and lower operational reliability (high waves are an additional weather hazard) compared to land-based aircraft. However, recent technological advances in materials and computational capabilities along with macroeconomic and ecological considerations may render this type of aircraft interesting. Point-to-point operation in coastal area could alleviate traffic congestion in urban airports and make remote islands more accessible. This, in turn, should help more balanced economic growth and better emergency services in smaller cities and rural areas. This paper addresses one of the drawbacks of seaplanes called porpoising, which is a dynamic instability in planing seaplanes and high-speed boats [1].

Porpoising is a coupled oscillatory motion between heaving and pitching that can manifest when seaplanes are travelling on water at planing speed (Fig. 1). This motion may become unstable and can pose significant risk to the safe operation of waterborne aircraft. Traditionally, the rules of thumb in the designing of hulls and physical experiments [2–5] (combined with pilot training [6,7]) have been the methods of mitigating the risk. However, the phenomenon is poorly understood and sufficient parametric studies applicable to seaplanes have not appeared in the literature. Current research aims to fill this gap. The objective is to effectively mitigate or eliminate porpoising by design.

Towing tank experiments [8] showed that moving the center of gravity aft, or employing flexible supports (between the aircraft and the floats), could improve the stability of the planing craft (Fig. 2). To understand these observations, linear-time-invariant models were constructed and the stability of oscillatory motions was studied. The

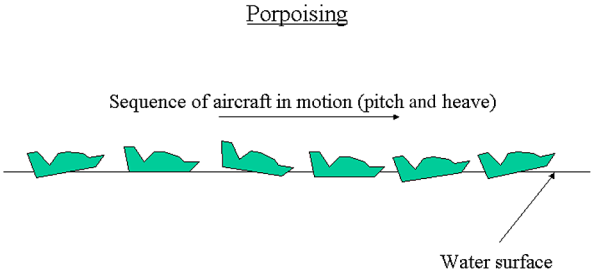

Fig. 1 Schematic of porpoising.

Fig. 2 Implementation of the flexible support system in an ultralight plane.

Fig. 3 Experiment with the flexible support at the towing tank of Yokohama National University.

numerical models were coherent with the experiments and two major design questions were answered, namely, 1) whether the appropriate direction to move the center of gravity is forward or backrward when porpoising is a problem [9], and 2) whether flexible supports suppress porpoising globally or under certain conditions.

In the literature, most of the work investigating the longitudinal stability of planing seaplanes is experimental. A large portion of them was conducted before the prevalence of fast, personal computers (i.e., before the 1970 s). The parametric investigation of porpoising behavior based on numerical simulations and investigation of flexible supports for the mitigation of porpoising are two contributions of this work.

II. Methods

The first step in this study is to numerically recreate, at least qualitatively, the observation made in the towing tank experiments. Particularly, the objective here is to confirm that the inception of porpoising occurs at approximately 5 m/s of the towing speed with the original center-of-gravity (CG) location and that moving the CG aft stabilizes the towed model. Then, we would like to observe numerically that the flexible support "stabilizes" the towed model. The second step is to explore different designs by varying parameters in the numerical model. The towed model consists of a pair of floats in a catamaran configuration and a frame on top of them (Fig. 3). The frame has adjustable weights to roughly simulate the inertia characteristics of the aircraft that the float is designed for, which is a 1/3-scale Piper Cub. By changing the location of weights, one can also move the location of the CG backward or forward. In the following, the numerical model of the conventional rigid case and then the flexibly supported case are described.

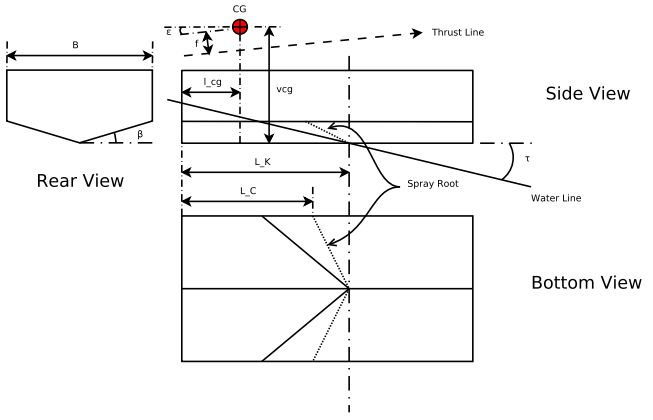

Fig. 4 Diagram of planing hull cutout.

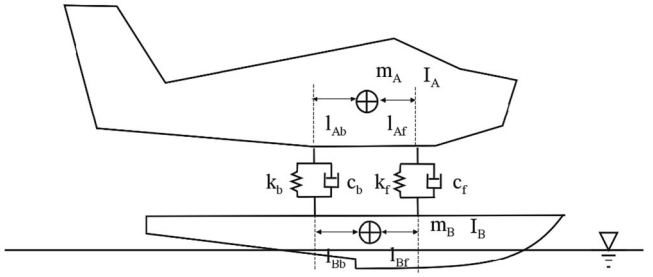

Fig. 5 Schematic of a float plane with the flexible support.

For the numerical analysis, the catamaran configuration was replaced by a monohull representation of the prismatic hull, as shown in Fig. 4. The transom location in this figure corresponds to the step location in the actual float. The afterbody of the float was neglected in the modeling, and so was the curved front portion of the forebody of the float. Figure 5 shows the schematic of the system to be modeled. The dynamic stability was computed using a small perturbation analysis, as presented in the work by Faltinsen [10]. The coordinate systems employed are shown in Fig. 6. For the rigidly supported case, the inertial coordinate system x_b, z_b was set to move along with the towed craft; its origin coincides with the equilibrium position of the craft's center of gravity. The x axes point to the stern of the craft. For the flexibly supported case, separate inertial coordinate systems that move along the craft were employed for above the support x_a, z_a and the float x_b, z_b. These were an approximate way to represent the dynamics (for the frame had a surge component of motion that was neglected) but were done in order to facilitate the analysis. The linear system of equation for the rigidly supported case is Eq. (1) and, for the flexibly supported case, Eq. (2). The added mass A_{ij}, damping force coefficient B_{ij}, and restoring force coefficient C_{ij} were formulated according to chapters 8 and 9 of Faltinsen's book [10]. A cursory description of how A_{ij}, B_{ij}, and C_{ij} were computed is given in the appendices. The numbers in subscripts ($i, j \in \{3, 5\}$) denote heaving 3 and pitching 5, respectively. The first subscript i refers to the resulting force or moment direction, and the second subscript j refers to the motion causing the force or moment. For example, C_{35} refers to the heaving force coefficient due to pitching motion. One can also find relevant information on the hydrodynamic forces for planing crafts in [9,11–13].

The flexibly supported case contains additional parameters on the characteristics of the support, namely, the spring constants k_f and k_b, as well as the damping coefficients c_f and c_b. The subscripts denote their locations: f for front, and b for back. Likewise, the attachment locations relative to center of gravity are denoted as l_{Af} and l_{Ab} for the front and back attachment points on the aircraft side, respectively; and l_{Bf} and l_{Bb} denote the front and back attachments on the float side. These parameters are visualized in Fig. 5. We have kept the attachment points fixed and varied the spring constants and damping coefficients in our numerical simulations.

In the rigidly supported case, we also used self-organizing map-based adaptive sampling (SOMBAS) [14,15] to search for

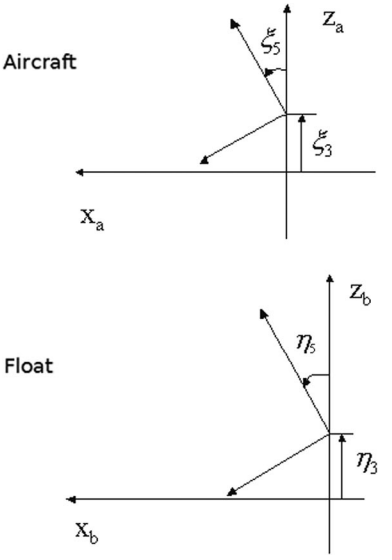

Fig. 6 Coordinate system for the small perturbation method.

stable designs. SOMBAS is suitable for the task of searching for multiple and diverse solutions satisfying certain objective conditions. We searched for designs with negative values in the maximum real part of the eigenvalues. For the two-design-variable case, we used the longitudinal distance of the CG along the keel line l_{cg} measured from the step or transom and the vertical distance of the CG from the keel line vcg. For the seven-design-variable case, we used the beam length B, the deadrise angle β_{deg}, the pitching moment of inertia I_{55}, the thrust line distance f from the CG (positive when pitchup moment results), and the thrust line angle with respect to the keel line (positive upward) ϵ. Figure 4 shows a diagram describing the design variables, except the inertial variable I_{55}.

$$\begin{pmatrix} M + A_{33} & A_{35} & 0 & 0 \\ A_{53} & I_{55} + A_{55} & 0 & 0 \\ 0 & 0 & 1 & 0 \\ 0 & 0 & 0 & 1 \end{pmatrix} \begin{pmatrix} \ddot{\eta}_3 \\ \ddot{\eta}_5 \\ \dot{\eta}_3 \\ \dot{\eta}_5 \end{pmatrix} + \begin{pmatrix} B_{33} & B_{35} & C_{33} & C_{35} \\ B_{53} & B_{55} & C_{53} & C_{55} \\ -1 & 0 & 0 & 0 \\ 0 & -1 & 0 & 0 \end{pmatrix} \begin{pmatrix} \dot{\eta}_3 \\ \dot{\eta}_5 \\ \eta_3 \\ \eta_5 \end{pmatrix} = \begin{pmatrix} 0 \\ 0 \\ 0 \\ 0 \end{pmatrix} \tag{1}$$

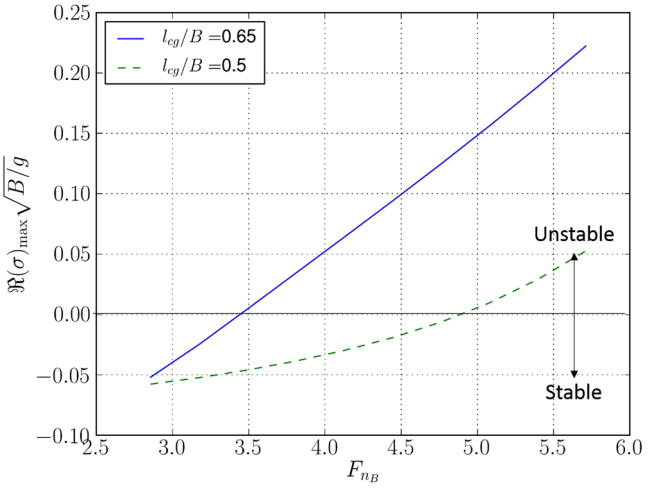

Fig. 7 Porpoising mitigation by moving the CG aft.

$$
\begin{pmatrix}
m_A & 0 & 0 & 0 & 0 & 0 & 0 & 0 \\
0 & I_A & 0 & 0 & 0 & 0 & 0 & 0 \\
0 & 0 & 1 & 0 & 0 & 0 & 0 & 0 \\
0 & 0 & 0 & 1 & 0 & 0 & 0 & 0 \\
0 & 0 & 0 & 0 & m_B + A_{33} & A_{35} & 0 & 0 \\
0 & 0 & 0 & 0 & A_{53} & I_B + A_{55} & 0 & 0 \\
0 & 0 & 0 & 0 & 0 & 0 & 1 & 0 \\
0 & 0 & 0 & 0 & 0 & 0 & 0 & 1
\end{pmatrix}
\begin{pmatrix} \ddot{\xi}_3 \\ \ddot{\xi}_5 \\ \dot{\xi}_3 \\ \dot{\xi}_5 \\ \ddot{\eta}_3 \\ \ddot{\eta}_5 \\ \dot{\eta}_3 \\ \dot{\eta}_5 \end{pmatrix}
+
\begin{pmatrix}
c_f + c_b & c_f l_{Af} - c_b l_{Ab} & k_f + k_b & k_f l_{Af} - k_b l_{Ab} & -c_f - c_b & -c_f l_{Bf} + c_b l_{Bb} & -k_f - k_b & -k_f l_{Bf} + k_b l_{Bb} \\
c_f l_{Af} - c_b l_{Ab} & c_f l_{Af}^2 + c_b l_{Ab}^2 & k_f l_{Af} - k_b l_{Ab} & k_f l_{Af}^2 + k_b l_{Ab}^2 & -c_f l_{Af} + c_b l_{Ab} & -c_f l_{Af} l_{Bf} - c_b l_{Ab} l_{Bb} & -k_f l_{Af} + k_b l_{Ab} & -k_f l_{Af} l_{Bf} - k_b l_{Ab} l_{Bb} \\
-1 & 0 & 0 & 0 & 0 & 0 & 0 & 0 \\
0 & -1 & 0 & 0 & 0 & 0 & 0 & 0 \\
-c_f - c_b & -c_f l_{Af} + c_b l_{Ab} & -k_f - k_b & -k_f l_{Af} + k_b l_{Ab} & B_{33} + c_f + c_b & B_{35} + c_f l_{Bf} - c_b l_{Bb} & C_{33} + k_f + k_b & C_{35} + k_f l_{Bf} - k_b l_{Bb} \\
-c_f l_{Bf} + c_b l_{Bb} & -c_f l_{Af} l_{Bf} - c_b l_{Ab} l_{Bb} & -k_f l_{Bf} + k_b l_{Bb} & -k_f l_{Af} l_{Bf} - k_b l_{Ab} l_{Bb} & B_{53} + c_f l_{Bf} - c_b l_{Bb} & B_{55} + c_f l_{Bf}^2 + c_b l_{Bb}^2 & C_{53} + k_f l_{Bf} - k_b l_{Bb} & C_{55} + k_f l_{Bf}^2 + k_b l_{Bb}^2 \\
0 & 0 & 0 & 0 & -1 & 0 & 0 & 0 \\
0 & 0 & 0 & 0 & 0 & -1 & 0 & 0
\end{pmatrix}
\begin{pmatrix} \dot{\xi}_3 \\ \dot{\xi}_5 \\ \xi_3 \\ \xi_5 \\ \dot{\eta}_3 \\ \dot{\eta}_5 \\ \eta_3 \\ \eta_5 \end{pmatrix}
=
\begin{pmatrix} 0 \\ 0 \\ 0 \\ 0 \\ 0 \\ 0 \\ 0 \\ 0 \end{pmatrix}
\tag{2}
$$

III. Results

Figures 7–9, 14, and 15 are for the rigidly supported case; and Figs. 10–13 are for the flexibly supported case. Nominal conditions for the calculation are as following unless otherwise specified: the planing speed is $U = 6.0$ m/s; the mass of the craft for the rigid case is $M = 16.18$ kg and for the flexible case is $m_A = 10.79$ kg (aircraft); $m_B = 5.39$ kg (float); the beam length is $B = 0.2$ m; the moment of inertia for the rigid case is $I_{55} = 5.981$ kg $\cdot$ m^2 and for the flexible case is $I_A = 4.351$ kg $\cdot$ m^2 (aircraft); $I_B = 1.630$ kg $\cdot$ m^2 (float); the length along the keel from the step to the center of gravity is $l_{\mathrm{cg}} = 0.104$ m; the distance of the CG from the keel is $v_{\mathrm{cg}} = 0.453$ m; and the moment arm length from the CG to the supports (Fig. 5) is $l_{Af} = l_{Ab} = l_{Bf} = l_{Bb} = 0.2$ m. The Froude number is defined based on the beam length $F_{n_B} = U/\sqrt{gB}$. The beam length B and l_{cg} are not reported in Hirakawa et al.'s paper [8], and the values reported above are educated guesses. In the simulation, we use the half-body representation. That means we halve the mass and moment of inertia in the calculations, and we model them as a monohull float plane.

For plots with vertical axes showing the maximum eigenvalue $\mathcal{R}(\sigma)_{\max}$ of the linear system, any positive value of the real part of the eigenvalue signifies divergence of the oscillation mode, and therefore is unstable. The eigenvalues are calculated from the matrix obtained in the following way. $\boldsymbol{K} = \mathbf{M}^{-1}(-\mathbf{R})$, where $\mathbf{M}\dot{\boldsymbol{x}} + \mathbf{R}\boldsymbol{x} = 0$ and $\boldsymbol{x}$ is the state vector and where $\mathbf{M}$ and $\mathbf{R}$ represent the matrices in Eqs. (1) and (2).

Figure 7 confirms that moving the CG backward toward the step helps the craft to remain stable until a higher velocity. The figure shows the maximum real part of the eigenvalues $\mathcal{R}(\sigma)_{\max}\sqrt{B/g}$ with respect to the Froude number F_{n_B}. We kept the beam length B constant. Thus, the Froude number is essentially a non-dimensionalized speed. In the towing tank experiment, divergence (porpoising) occurred at about $U = 5.0$ m/s [8] ($F_{n_B} = 3.57$) with the nominal l_{cg}/B location of 5.2. Figure 7 shows that, in the numerical simulation, planing craft with $l_{\mathrm{cg}}/B = 0.50$ turn unstable at just under $F_{n_B} = 5.0$ and, with $l_{\mathrm{cg}}/B = 0.65$, turn unstable at just under $F_{n_B} = 3.5$. Note that, in the physical dimensions, the two l_{cg} values differ only by 0.03 m (or 1.95% of the float length of 1.54 m [8]) and the speed limit for stable planing changes by 2.10 m/s (or 42.8% difference). Thus, the planing speed U at which the craft turns unstable is very sensitive to the CG location. Considering the fact that values for B and l_{cg} are only approximately known, the numerical results are very reasonable in light of the experimental evidence.

The trim angles τ corresponding to the two l_{cg} values with respect to F_{n_B} are shown in Fig. 8. The trim angles are found by driving the moment equation to have a near-zero residue moment. This is done

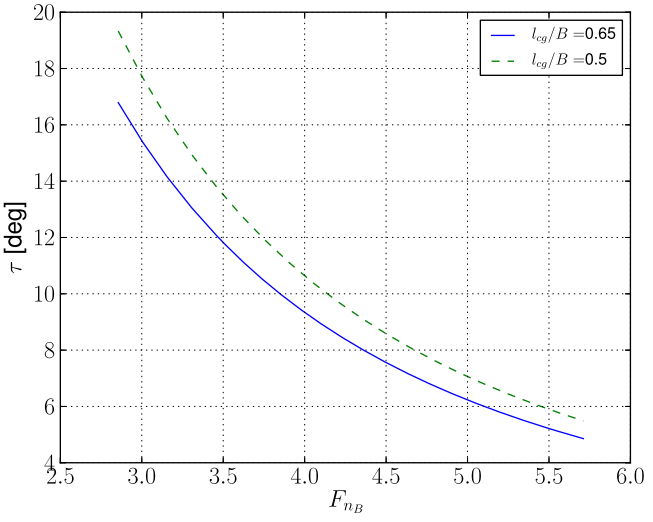

Fig. 8 Trim angle of the simulated model with respect to the Froude number F_{n_B}.

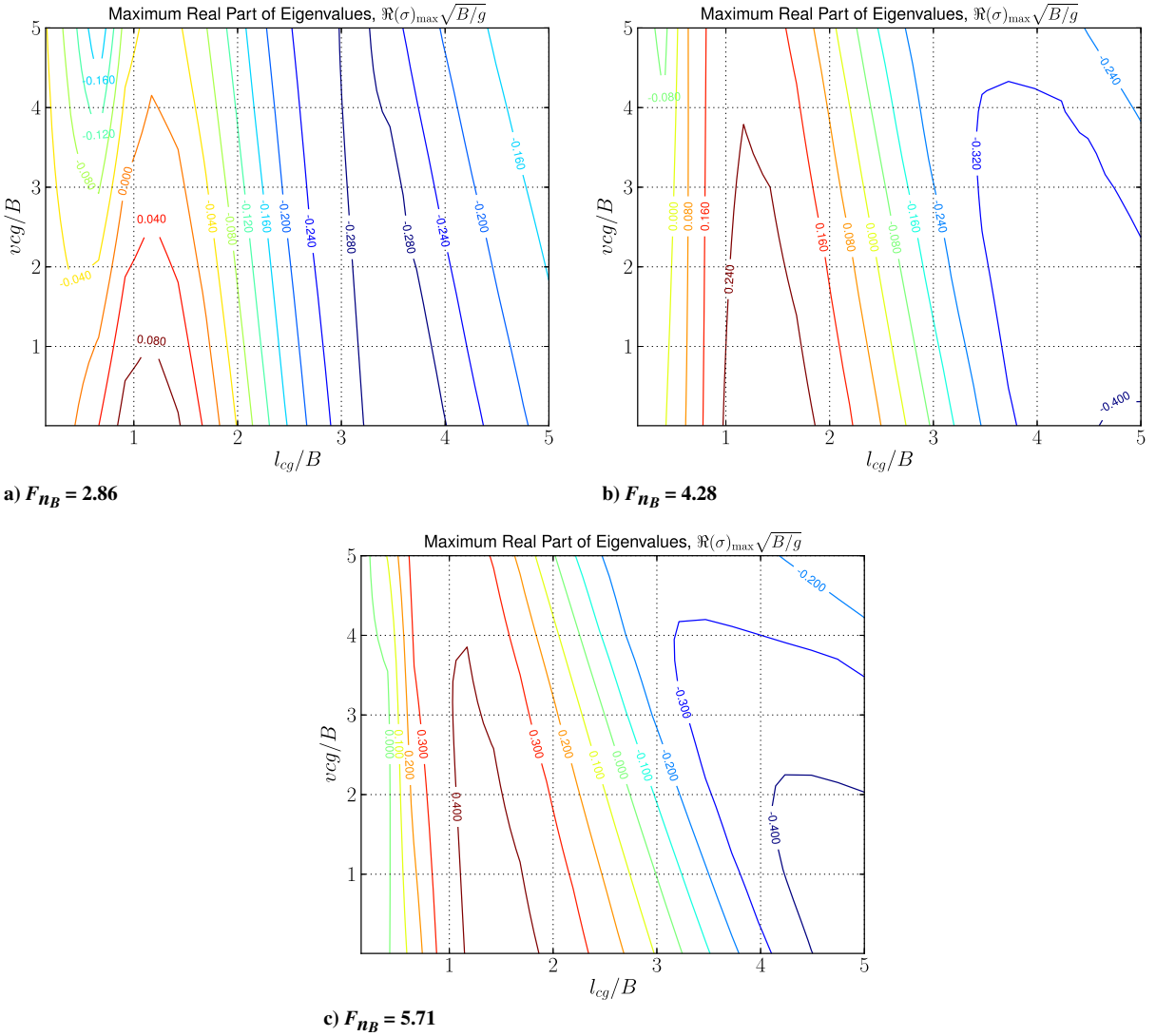

Fig. 9 Stability with respect to l_{cg} and v_{cg}. $\mathcal{R}(\sigma)_{\max}\sqrt{B/g} < 0$ are stable designs.

using Brent's method ([16] chaps. 3–4) implemented in the SciPy optimize module of the Python programming language. One can let the solutions have small residues so that the trim angles found can be used as a small perturbation in the subsequent eigenvalue computations.

Figure 9 indicates that the desirable direction of moving the CG (i.e., forward or backward) to stabilize an unstable planing condition depends on the current value of l_{cg}. There is a band of l_{cg} values at which a nondecaying oscillation manifests with positive $\mathcal{R}(\sigma)_{\max}\sqrt{B/g}$. This band of instability increases in width as F_{n_B} increases from 2.86 to 5.71, as seen in Figs. 9a–9c. The contour plots show that the sensitivity of the stability to changes in vcg is not as marked as changes in l_{cg}. A small portion of the design space near the transom or very small value of l_{cg} generates stable designs, and most float planes have this configuration to facilitate the pitchup at the moment of takeoff. This means that, to make the planing stable, it is a good idea to shift the CG aft. However, once airborne, it is better to have the CG forward to have enough "static margin" for a stable flight.

Figure 10 checks whether the two simulation codes, one for the rigid-body case and the other for the flexibly supported case, agree if the flexible support's spring were extremely stiff. The plot shows $\mathcal{R}(\sigma)_{\max}\sqrt{B/g}$ with respect to F_{n_B}. The two lines agree very well.

Figures 11–13 show the effectiveness of the flexible support in mitigating unstable oscillations. However, as can be noted from the sharp rise in the real part of eigenvalues at high Froude numbers, it is not a globally stabilizing solution. Inadequate damping in the flexible supports can worsen the stability of the seaplane when compared with the conventional rigidly supported ones, as seen in Fig. 11a or Fig. 11b. This suggests that the damper should be designed carefully

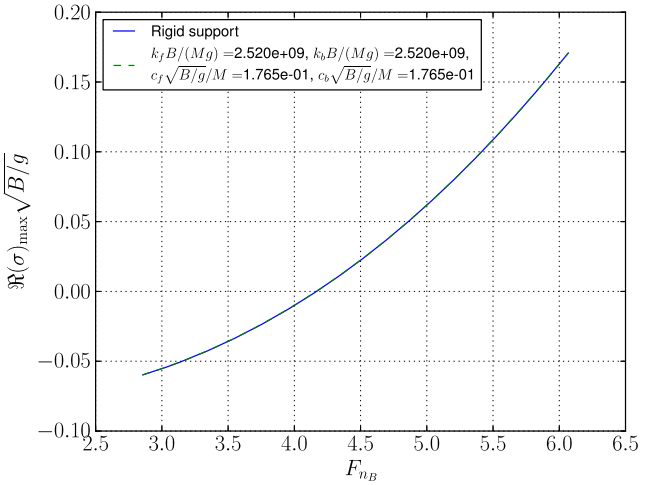

Fig. 10 Stability in the rigid-body and the flexible-support formulation with very stiff springs.

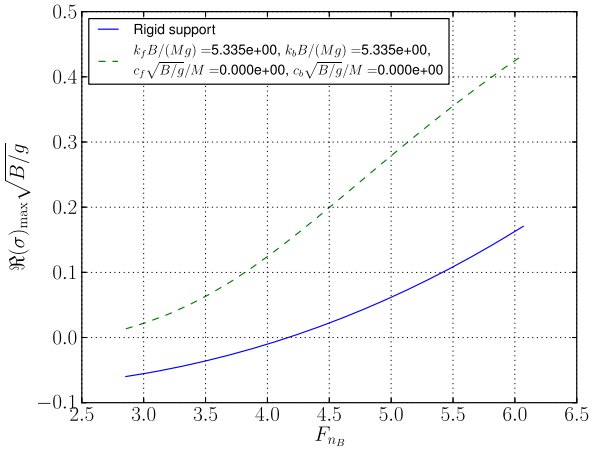

a) No damping

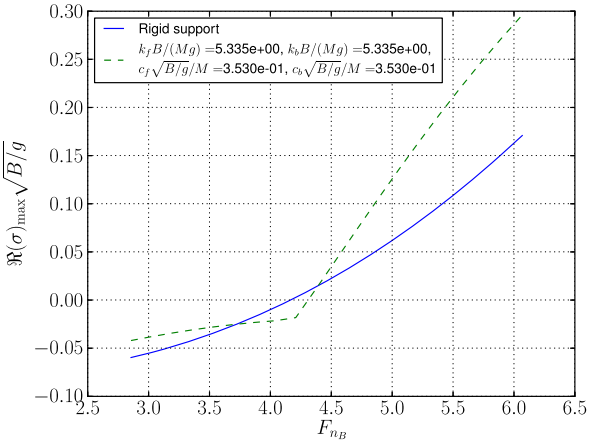

b) $c_{f,b}$ = 20 [N·s/m]

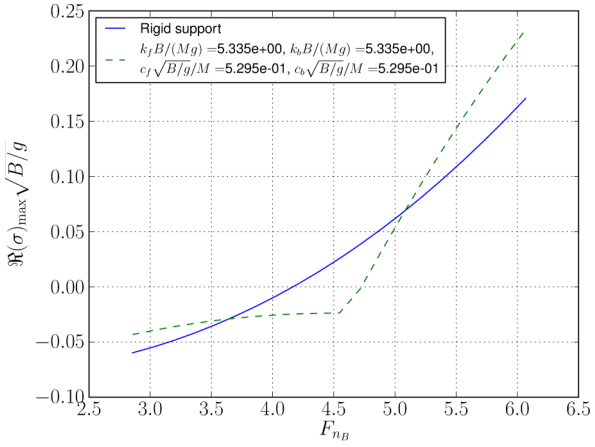

c) $c_{f,b}$ = 30 [N·s/m]

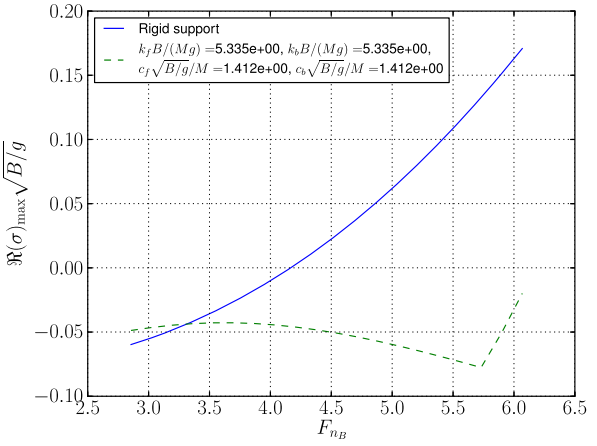

d) $c_{f,b}$ = 80 [N·s/m]

Fig. 11 Effect of damping in longitudinal stability of the flexibly supported case.

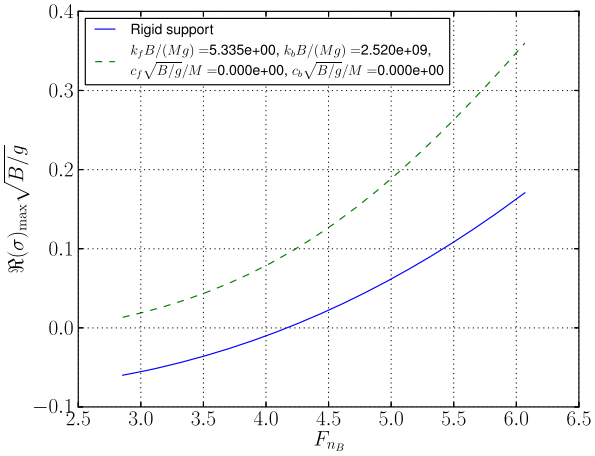

a) Flexible front support, no damping

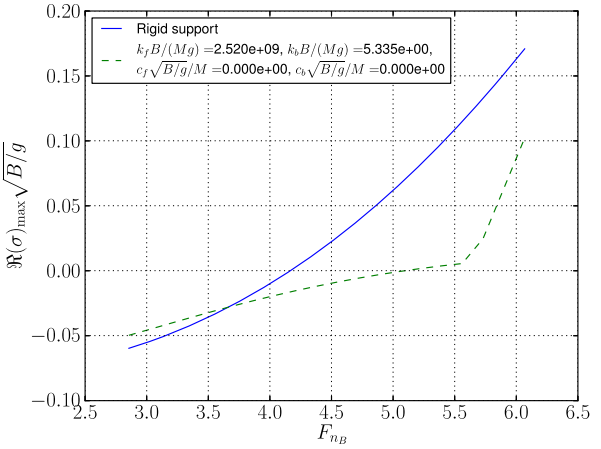

b) Flexible back support, no damping

Fig. 12 Longitudinal stabilities when only the front or the back suppot is flexible.

in such a way that no divergent oscillation modes occur in the planing speeds of the aircraft. Figure 12 shows that, if only one of either the front or back supports is made flexible, it is the back support that is effective in mitigating instabilities. Similarly, if damping is applied to either the front or the back support (that are both flexible), it is the damping of the back support that is more effective (Fig. 13). These results show some similarity with the flutter stability phenomena in aeroelasticity, in which the elastic axis location of the wing affects the divergence speed.

Figure 14 shows a contour plot of $\mathcal{R}(\sigma)_{\max}\sqrt{B/g}$ with respect to l_{cg} and vcg along with sampled points by SOMBAS in the two-design-variable case. SOMBAS was set to search feasible designs requiring $\mathcal{R}(\sigma)_{\max} < 0$. The sampled points that satisfied that condition are shown along with the final location of the training samples for the self-organizing map. The distribution of the training samples indicates the finite sample representation of the feasible region around which further sampling in the subsequent iterations are expected produce further space filling effects of the feasible design

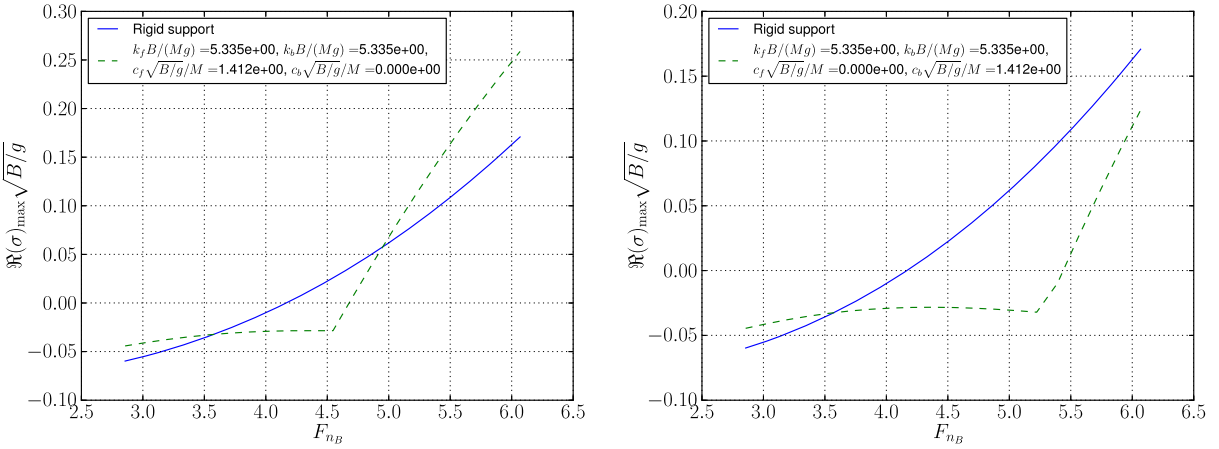

a) Applying damping only to the front support **b) Applying damping only to the back support**

Fig. 13 Longitudinal stabilities when only the front or the back support has damping.

space, i.e., further stable designs. In this trivial case (because we already have the contour plot), we see that SOMBAS sampled diverse combinations of l_{cg} and v_{cg} filling out the stable domain. This feasible region search capability is useful when the design space is in higher dimensions (many design variables) and full-factorial design (or grid sampling) becomes too expensive.

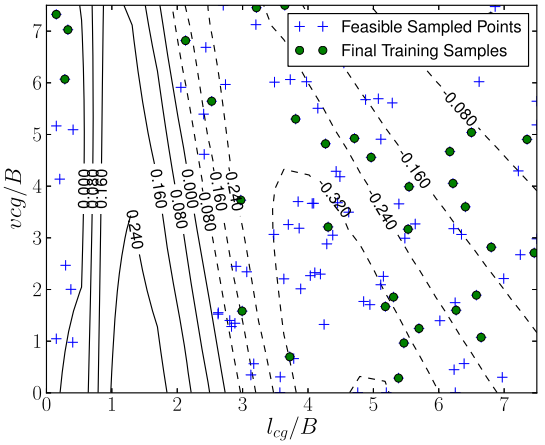

Fig. 14 SOMBAS sampling stable combinations of l_{cg} and vcg at $F_{n_B} = 4.28$.

Figure 15a shows the scatter plot matrix of the seven-design-variable case. N_f is the number of designs (experiments) computed by SOMBAS, and N_s is the number designs that satisfy the condition, i.e., $\mathcal{R}(\sigma)_{\max} < 0$. The lower triangular cells show the absolute values of correlation coefficients. Again, it clearly shows the unstable "band" for l_{cg} at the top row of the scatter plot matrix. The other parameter does not show clear unfeasible regions. Further restriction was applied by setting $\mathcal{R}(\sigma)_{\max} < -0.3$, and the results are shown in Fig. 15b. It shows some new trends. For example, vcg tends to a lower value as the eigenvalue becomes more negative. On the other hand, the beam length B tends to a larger value as the eigenvalue becomes more negative. The l_{cg} concentrates between 0.8 and 1.2, and vcg tends to low values as l_{cg} becomes longer.

IV. Discussions

It is desirable to conduct further experiments to improve the quality of the model by calibration and further numerical model refinement. The hull geometry and the flexible-support model employed in this research were very simple. Inclusion of the afterbody of the float (the portion after the step) may create another planing surface at larger pitch angles, and this may create another instability. Further sophistication in the flexible-support model, including their control, may render further insights and new opportunities.

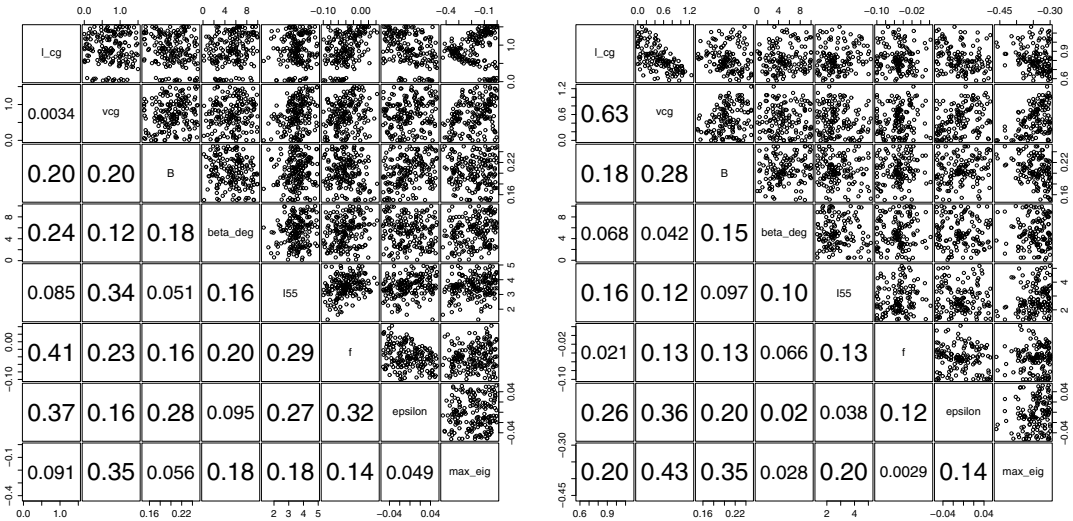

a) Maximum eigenvalues of oscillation modes less than 0, (N_f = 289, N_s = 181)

b) Maximum eigenvalues of oscillation modes less than -0.3, (N_f = 504, N_s = 135)

Fig. 15 Scatter matrix showing distribution of feasible designs at $F_{n_B} = 4.28$.

In the current study, the CG location (l_{cg} and vcg) and the pitching moment of inertia ($I_{55}, I_{A,B}$) were treated independently. However, in reality, they are not. Thus, care must be taken to interpret the results in this paper where both variables are treated independently.

In this paper, the aerodynamic effects were not considered. However, seaplanes receive substantial lift force at planing speeds and the elevator provides a means to control the pitch angle. Thus, the aerodynamics may have a substantial effect on the planing characteristics of a seaplane. The inclusion of the aerodynamic effects will be the next step in the development of the numerical simulation of the planing seaplanes.

Active and semiactive controls of the flexible support [17] can be considered to obtain a desired dynamics in both waveless and wavy conditions. For example, skyhook methods in which damping is controlled to emulate the dynamics of bodies for which the damper is attached to an imaginary inertial frame (hence skyhook), could be employed. This may be effective in eliminating porpoising, as well as improving operational reliability in wavy conditions. Of course, it comes at the cost of added weight and complexities.

Once validated, the parametric models (flexible or rigid) equip us with the means to conduct various tradeoff studies concerning porpoising at early design stages. These should provide more informed design decisions than the rules of thumb hitherto available. With the inclusion of aerodynamic forces, they will be useful in assessing the sizing, location, and incidence angles of the lifting surfaces with respect to planing hulls, as well as whether the flexible support will be needed. Eventually, a new set of design standards can be drawn concerning longitudinal stability of waterborne seaplanes, including the design of the flexible support.

V. Conclusions

The numerical analysis of the linear-time-invariant model revealed useful information to the questions posed. The computation showed that whether one should move the center of gravity backward or forward would depend on the position of the center of gravity with respect to the step of the planing hull. If a flexible support was employed, one might postpone the inception of porpoising to a much higher Froude number. The simulation results indicated that damping coefficients in the flexible supports played an important role and the range of the planing speed would determine their values. The damping in the hind support was more effective than the damping in the front support. These numerical results could be used to conduct more dedicated physical experiments to quantitatively assess the numerical models and confirm physical phenomena. Furthermore, aerodynamic effects must be taken into account. These will constitute the future work of this study, along with the parametric optimization of the system.

Appendix A: Overview of Hydrodynamic Calculations

The computation of stability takes two steps. First, the equilibrium or the trim position needs to be found given the planing speed. Second, the small perturbation analysis is performed about the equilibrium position by looking at the increments in the force and moment with respect to change in the state vector variables. As in flight dynamics, the stability derivatives need to be obtained about this equilibrium point. We will follow closely the procedure given by Falinsen [10]. A big part of the following is due to Savitsky [18] and Wagner [19].

Appendix B: Trim Determination

For trim determination, the following equilibria hold:
Vertical forces:

$$Mg = N\cos\tau + T\sin(\tau+\epsilon) - R_v\sin\tau \tag{B1}$$

Horizontal forces:

$$T\cos(\tau+\epsilon) = R_v\cos\tau + N\sin\tau \tag{B2}$$

Pitching moments:

$$Nc + R_v a - Tf = 0. \tag{B3}$$

N represents the resultant hydrodynamic pressure force (represented to be acting at a point along and perpendicular to the keel line in the vertical xz plane). T is the thrust force from the powerplant. These two forces can be expressed with respect to τ and R_v using Eqs. (B1) and (B2) (ϵ is given by the design). R_v is the frictional force exerted on the planning surface. Then, these can be plugged into moment force equation (B3) to obtain an equation of a, c, τ, and R_v (f is given by the design):

$$\frac{c}{\cos\tau}\left(Mg - \frac{Mg\sin\tau + R_v}{\cos\epsilon}\sin(\tau+\epsilon) + R_v\sin\tau\right) + R_v a - \frac{Mg\sin\tau + R_v}{\cos\epsilon}f = 0 \tag{B4}$$

The frictional force is given by

$$R_v = \frac{1}{2}\rho C_F S(U\cos\tau)^2 \simeq \frac{1}{2}\rho C_F S U^2 \tag{B5}$$

where ρ is water density, S is the wetted surface area, and C_F is the friction coefficient:

$$C_F = \frac{0.075}{(\log_{10}(R_n)-2)^2} + \frac{44[(\mathrm{AHR}/L_K)^{1/3} - 10R_n^{-1/3}] + 0.125}{10^3} \tag{B6}$$

where AHR is the average hull roughness in micrometers. We set the AHR to 150 μm. R_n is the Reynolds number based on the characteristic length L_K, which is the wetted keel length. The wetted area S is given as follows:

$$S = \frac{\tan^2\beta}{\sin\beta}\frac{B^2}{4(1+z_{\max}/Vt)\tau} + \frac{B}{\cos\beta}L_C \tag{B7}$$

where $1 + z_{\max}/Vt \simeq \pi/2$ for small β [for large β, see ([10] p. 303)], and L_C is the wetted chine length. Note that R_v is a function of τ, L_K, and L_C, which we do not know. The two moment arm lengths, a and c, pertaining to the hull frictional force R_v and hydrodynamic pressure force N, respectively, can be formulated as follows:

$$a = \mathrm{vcg} - \frac{B}{4}\tan(\beta) \tag{B8}$$

$$c = l_{cg} - l_p \tag{B9}$$

Then, a is fixed once CG location, B, and β are given, but to get c, we need to determine the distance of the center of hydrodynamic pressure from the step l_p. To determine l_p, we take three steps. First, we determine C_{L_0} using

$$C_{L_\beta} = \frac{F_{L_\beta}}{0.5\rho U^2 B^2} = C_{L_0} - 0.0065\beta_{\deg}C_{L_0}^{0.60} \tag{B10}$$

where $F_{L_\beta} = Mg$. Second, given F_{n_B}, we can obtain λ_W from

$$C_{L_0} = \frac{F_{L_0}}{0.5\rho U^2 B^2} = \tau_{\deg}^{1.1}\left[0.012\lambda_W^{0.5} + 0.0055\frac{\lambda_W^{2.5}}{F_{n_B}^2}\right] \tag{B11}$$

Again, we do not know the value for $\tau_{\deg}$. Thus, we temporarily assume some value for $\tau_{\deg}$. Third, the following equation gives l_p:

$$\frac{l_p}{\lambda_W B} = 0.75 - \frac{1}{(5.21F_{n_B}^2/\lambda_W^2) + 2.39} \tag{B12}$$

With the λ_W computed using assumed $\tau = \pi\tau_{\text{deg}}/180$, we can also obtain L_K and L_C from

$$\lambda_W = \frac{L_K + L_C}{2B} \tag{B13}$$

$$\frac{B}{2} = \frac{\pi}{2\tan\beta}(L_K - L_C)\tau \tag{B14}$$

These enable us to compute R_v for the assumed τ. We now check to see if Eq. (B4) holds. We iterate the process using Brent's method [16] until we find a good τ.

Appendix C: Stability Derivatives

Based on the trim condition obtained for a given planing speed U, we can now proceed to the calculation of the stability derivatives. The restoring force coefficients due to heave C_{33} and pitch C_{35} are given by

$$\frac{C_{33}}{0.5\rho U^2 B} = -B\frac{\partial C_{L_\beta}}{\partial\eta_3}\bigg|_0 = -B\frac{\partial C_{L_0}}{\partial\eta_3}\bigg|_0 [1 - 0.0039\beta_{\text{deg}}C_{L_0}^{-0.4}] \tag{C1}$$

$$\frac{C_{35}}{0.5\rho U^2 B} = -B\frac{\partial C_{L_\beta}}{\partial\eta_5}\bigg|_0 = -B\frac{\partial C_{L_0}}{\partial\eta_5}\bigg|_0 [1 - 0.0039\beta_{\text{deg}}C_{L_0}^{-0.4}] \tag{C2}$$

where $|_0$ denotes "at the static equilibrium position" and

$$\frac{\partial C_{L_0}}{\partial\eta_3}\bigg|_0 = \tau_{\text{deg}}^{1.1}\left[0.006\lambda_0^{-0.5} + \frac{0.01375\lambda_0^{1.5}}{F_{n_B}^2}\right]\frac{\partial\lambda_W}{\partial\eta_3}\bigg|_0 \tag{C3}$$

$$\frac{\partial C_{L_0}}{\partial\eta_5}\bigg|_0 = 1.1\left(\frac{180}{\pi}\right)^{1.1}\tau^{0.1}\left[0.012\lambda_0^{0.5} + \frac{0.0055\lambda_0^{2.5}}{F_{n_B}^2}\right]$$

$$+\tau_{\text{deg}}^{1.1}\left[0.006\lambda_0^{-0.5} + \frac{0.01375\lambda_0^{1.5}}{F_{n_B}^2}\right]\frac{\partial\lambda_W}{\partial\eta_5}\bigg|_0 \tag{C4}$$

Here, λ_0 is the value of λ_W at the static equilibrium. Furthermore,

$$\frac{\partial\lambda_W}{\partial\eta_3}\bigg|_0 = -\frac{1}{\sin\tau}\frac{1}{B} \tag{C5}$$

$$\frac{\partial\lambda_W}{\partial\eta_5}\bigg|_0 = \frac{-\text{vcg}/B}{\sin^2\tau} + \frac{z_{wl}/B}{\sin^2\tau}\cos\tau + \frac{0.25\tan\beta}{(1 + z_{\max}/Vt)\tau^2} \tag{C6}$$

From Eq. (B12), we can write

$$\frac{1}{B}\frac{\partial l_p}{\partial\lambda_W}\bigg|_0 = 0.75 - \frac{15.63(F_{n_B}^2/\lambda_0^2) + 2.39}{(5.21(F_{n_B}^2/\lambda_0^2) + 2.39)^2} \tag{C7}$$

Then, we can compute the pitch moment coefficients due to heaving C_{53} and due to pitching C_{55} as

$$\frac{C_{53}}{0.5\rho U^2 B^2} = -\left[\frac{1}{B}\frac{\partial l_p}{\partial\lambda_W}B\frac{\partial\lambda}{\partial\eta_3}C_{L_\beta} + \left(\frac{l_p}{B} - \frac{l_{\text{cg}}}{B}\right)B\frac{\partial C_{L_\beta}}{\partial\eta_3}\right]_0 \tag{C8}$$

$$\frac{C_{55}}{0.5U^2 B^3} = -\left[\frac{1}{B}\frac{\partial l_p}{\partial\lambda_W}\frac{\partial\lambda_W}{\partial\eta_5}C_{L_\beta} + \left(\frac{l_p}{B} - \frac{l_{\text{cg}}}{B}\right)\frac{\partial C_{L_\beta}}{\partial\eta_5}\right]_0 \tag{C9}$$

The added mass calculations are divided into two hull regions: the region where the keel is wet but the chine is not (the triangular planform region), and the region thereafter up to the step where the planing surface is completely wet (the rectangular planform region). The strip theory is used to exploit two-dimensional analytical solutions. A two-dimensional added mass of a wedge can be given using a Gamma function:

$$a_{33} \equiv \rho d^2 K = \frac{\rho d^2}{\tan\beta}\left[\frac{\pi}{\sin\beta}\frac{\Gamma(1.5 - \beta/\pi)}{\Gamma^2(1 - \beta/\pi)\Gamma(0.5 + \beta/\pi)} - 1\right] \tag{C10}$$

where d is the draft, and we only consider the real part of K. Then, d is defined as the draft from the spray root position:

$$d = \left(1 + \frac{z_{\max}}{Vt}\right)x\tau \tag{C11}$$

Here, x is on the axis that increases toward the step along the keel line, with the origin at the point where the wetting of the keel starts. In particular, we denote x_s as the point at which chine wetting starts. The added mass in the heaving of the triangular region is obtained from

$$A_{33}^{(1)} = \rho K\left(1 + \frac{Z_{\max}}{Vt}\right)\tau^2\int_0^{x_s} x^2\,\mathrm{d}x \tag{C12}$$

where

$$x_s = \frac{B}{2}\frac{\tan\beta}{(1 + (Z_{\max}/Vt))\tau} \tag{C13}$$

After integration, we have

$$\frac{A_{33}^{(1)}}{\rho B^3} = \frac{K}{24}\frac{\tan^3\beta}{(1 + (Z_{\max}/Vt))\tau} \tag{C14}$$

For the pitch-induced added mass in the triangular region,

$$A_{35}^{(1)} = A_{53}^{(1)} = -\rho K\int_0^{x_s} d^2(x - x_G)\,\mathrm{d}x \tag{C15}$$

where $x_G = L_K - l_{\text{cg}}$. After integration, we obtain

$$\frac{A_{35}^{(1)}}{\rho B^4} = \frac{A_{53}^{(1)}}{\rho B^4} = \frac{A_{33}^{(1)}}{\rho B^3}\frac{x_G}{B} - \frac{K}{64}\frac{tan^4\beta}{(1 + (Z_{\max}/Vt))^2\tau^2} \tag{C16}$$

We also have

$$A_{55}^{(1)} = \rho K\int_0^{x_s} d^2(x - x_G)^2\,\mathrm{d}x \tag{C17}$$

which results in

$$\frac{A_{55}^{(1)}}{\rho B^5} = \frac{K}{160}\frac{\tan^5\beta}{(1+(Z_{\max}/Vt))^3\tau^3} - \frac{K}{32}\frac{x_G}{B}\frac{\tan^4\beta}{(1+(Z_{\max}/Vt))^2\tau^2} + \left(\frac{x_G}{B}\right)^2\frac{A_{33}^{(1)}}{\rho B^3} \tag{C18}$$

As for the rectangular region, the heaving induced part is given by

$$\frac{A_{33}^{(2)}}{\rho B^3} = C_1\frac{\pi}{8}\frac{L_C}{B} \tag{C19}$$

where

$$C_1 = \frac{2\tan^2\beta}{\pi}K \tag{C20}$$

The pitching-induced added masses of the rectangular portion are

$$\frac{A_{35}^{(2)}}{\rho B^4} = \frac{A_{53}^{(2)}}{\rho B^4} = -C_1\frac{\pi}{16}\left[\left(\frac{L_K}{B}\right)^2 - \left(\frac{x_s}{B}\right)^2\right] + \frac{x_G}{B}\frac{A_{33}^{(2)}}{\rho B^3} \tag{C21}$$

and

$$\frac{A_{55}^{(2)}}{\rho B^5} = \frac{C_1\pi}{24}\left(\left(\frac{L_K}{B}\right)^3 - \left(\frac{x_s}{B}\right)^3\right) - \frac{C_1\pi}{8}\left(\frac{x_G}{B}\right)\left(\left(\frac{L_K}{B}\right)^2 - \left(\frac{x_s}{B}\right)^2\right) + \left(\frac{x_G}{B}\right)^2\frac{A_{33}^{(2)}}{\rho B^3} \tag{C22}$$

The resulting added masses are given by $A_{ij} = A_{ij}^{(1)} + A_{ij}^{(2)}$.

The damping coefficients B_{ij} are analyzed using a quasi-steady approach in which changes in the angle of attack immediately cause changes in lift. We exclude hydrostatic effects in Eqs. (B10) and (B11) by setting $F_{n_B} \to \infty$:

$$C_{L_\beta} = C_{L_0} - 0.0065\beta_{\deg}C_{L_0}^{0.60} \tag{C23}$$

where

$$C_{L_0} = \left(\frac{180}{\pi}\right)^{1.1}\tau^{1.1}0.012\lambda_W^{0.5} \tag{C24}$$

Because of the heave velocity, there is a change in the angle of attack (trim):

$$\alpha = -\frac{\mathrm{d}\eta_3}{\mathrm{d}t}/U = -\frac{\dot{\eta}_3}{U} \tag{C25}$$

This causes a vertical force:

$$F_3 = -\frac{1}{2}\rho U^2B^2\frac{\partial C_{L_\beta}}{\partial\tau}\frac{\dot{\eta}_3}{U} \tag{C26}$$

where

$$\frac{\partial C_{L_\beta}}{\partial\tau} = \frac{\partial C_{L_0}}{\partial\tau}[1 - 0.0039\beta_{\deg}C_{L_0}^{-0.4}] \tag{C27}$$

and

$$\frac{\partial C_{L_0}}{\partial\tau} = 0.0132\left(\frac{180}{\pi}\right)^{1.1}\tau^{0.1}\lambda_W^{0.5} \tag{C28}$$

Note the $\dot{\eta}_3$ in Eq. (C26). This gives the heaving damping force:

$$\frac{B_{33}}{\rho B^3(g/B)^{1/2}} = 0.5F_{n_B}\frac{\partial C_{L_\beta}}{\partial\tau} \tag{C29}$$

The pitching moment resulting from the heave velocity can be computed using

$$F_5 = F_3(0.75\lambda_W B - l_{\mathrm{cg}}) \tag{C30}$$

and this gives

$$\frac{B_{53}}{B_{33}B} = 0.75\lambda_W - \frac{l_{\mathrm{cg}}}{B} \tag{C31}$$

The damping coefficients B_{55} and B_{35} are studied with respect to $\mathrm{d}\eta_5/\mathrm{d}t$ [20], and they are given as

$$B_{55} = Ux_T^2a_{33}(x_T) \tag{C32}$$

$$B_{35} = UA_{33} - Ux_Ta_{33}(x_T) \tag{C33}$$

where

$$a_{33}(x_T) = \rho\left(\frac{B\tan\beta}{2}\right)^2K \tag{C34}$$

is the two-dimensional added mass in heave for the cross section at step $x_T = l_{\mathrm{cg}}$.

Acknowledgment

Keiichi Ito has been funded by the Institute for the Promotion of Innovation through Science and Technology through the Baekeland Mandate program in the research and development of self-organizing map-based adaptive sampling. His research has also been funded by the Interuniversity Attraction Poles Programme BElgian Network on STochastic modelling, analysis, design and optimization of COMmunication systems (BESTCOM), initiated by the Belgian Science Policy Office. The undergoing project of developing innovative seaplanes (project managed by Tatsumi Sakurai, as well as the members of Hiyoh Aircraft Manufacturing and Development Company and Aeromarine Systems Cooperation Association) is an endeavor supported by many dedicated and enthusiastic volunteers.

References

[1] Stinton, D., "Aero-Marine Design and Flying Qualities of Floatplanes and Flying-Boats," *Aeronautical Journal*, Vol. 91, March 1987, pp. 97–127.

[2] Parkinson, J. B., "Appreciation and Determination of the Hydrodynamic Qualities of Seaplanes," NACA TN-1290, Washington, D.C., May 1947.

[3] Shuford, C. L., Jr., "A Theoretical and Experimental Study of Planing Surfaces Including Effects of Cross Section and Plan Form," NACA Rept. 1355, 1958.

[4] Garner, H. M., "Porpoising Test on a Model of a Flying Boat Hull," Marine Aircraft Experimental Establishment Reports and Memoranda 1492, Felixstowe, U.K., March 1932.

[5] Tomaszewski, K. M., "Hydrodynamic Design of Seaplane Floats," Current Papers, Ministry of Supply Aeronautical Research Council, Rept. No. Aero 2154, London, U.K., 1950.

[6] De Remer, D., *Water Flying Concepts: An Advanced Text on Wilderness Water Flying*, 2nd ed., Aviation Supplies and Academics, Newcastle, WA, 1990, pp. 9-1–9-14.

[7] Mees, B., *Notes of a Seaplane Instructor*, Aviation Supplies and Academics, Newcastle, WA, 1998, p. 10.

[8] Hirakawa, Y., Takayama, T., Kosaki, A., Kikuchi, H., Hirayama, T., and Sakurai, T., "Model Experiment of a Suppression-System for Wave Impact and Porpoising Phenomena," *Conference Proceedings of the Japan Society of Naval Architects and Ocean Engineers*, Vol. 3, The Japan Soc. of Naval Architects and Ocean Engineers, Tokyo, Japan, 2006, pp. 239–242 (in Japanese).

[9] Klemlin, A., Pierson, J. D., and Storer, E. M., "An Introduction to Seaplane Porpoising," *Journal of the Aeronautical Sciences*, Vol. 6, No. 8, June 1939, pp. 1905–1915.

[10] Faltinsen, O. M., *Hydrodynamics of High-Speed Marine Vehicles*, Cambridge Univ. Press, New York, 2005, pp. 302, 303, 342–372.

[11] Abrate, S., "Hull Slamming," *Applied Mechanics Reviews*, Vol. 64, No. 6, Nov. 2011, Paper 060803.

[12] Ikeda, Y., and Katayama, T., "Porpoising Oscillation of Very-High-Speed Marine Craft," *Philosophical Transactions of the Royal Society, Series A: Mathematical and Physical Sciences*, Vol. 358, No. 1771, 2000, pp. 1905–1915.
doi:10.1098/rsta.2000.0620

[13] Benson, J. M., and Freihofner, A., "Methods and Charts for Computing Stability Derivatives of a v-Bottom Planing Surface," NACA, Langley Memorial Aeronautical Lab. TR ARR-3L08, Hampton, VA, 1943.

[14] Ito, K., Dhaene, T., El Masri, N., d'Ippolito, R., and Van de Peer, J., "Self-Organizing Map Based Adaptive Sampling," *Proceedings of 5th International Conference on Experiments/Process/System Modeling/ Simulation/Optimization (5th IC-EpsMsO)*, Vol. 2, Learning Foundation in Mechatronics, Athens, Greece, July 2013, pp. 504–513.

[15] Ito, K., Couckuyt, I., d'Ippolito, R., and Dhaene, T., "Design Space Exploration Using Self-Organizing Map Based Adaptive Sampling," *Applied Soft Computing*, Vol. 43, June 2016, pp. 337–346.

[16] Brent, R. P., *Algorithms for Minimization Without Derivatives*, Prentice–Hall, Englewood Cliffs, NJ, 1973, pp. 19–60.

[17] Canale, M., Milanese, M., and Novara, C., "Semi-Active Suspension Control Using 'Fast' Model-Predictive Techniques," *IEEE Transactions on Control Systems Technology*, Vol. 14, No. 6, Nov. 2006, pp. 1034–1046.
doi:10.1109/TCST.2006.880196

[18] Savitsky, D., "Hydrodynamic Design of Planing Hulls," *Marine Technology*, Vol. 1, No. 1, Oct. 1964, pp. 71–96.

[19] Wagner, H., "Über Stoß- und Gleitvorgänge an der Oberfläche von Flüssigkeiten," *Zeitschrift für Angewandte Mathematik und Mechanik*, Vol. 12, No. 4, Aug. 1932, pp. 193–215 (in German).
doi:10.1002/(ISSN)1521-4001

[20] Salvesen, N., Tuck, E. O., and Faltinsen, O., "Ship Motions and Sea Loads," *SNAME Transactions*, Vol. 78, 1970, pp. 250–287.